Journal of Applied Electrochemistry **30**: 1243–1253, 2000.

Improvement of the high energy ball-milling preparation procedure of CO tolerant Pt and Ru containing catalysts for polymer electrolyte fuel cells

M.C. DENIS[1], P. GOUÉREC[1], D. GUAY[1], J.P. DODELET[1]*, G. LALANDE[2] and R. SCHULZ[2]
[1]*INRS-Énergie et Matériaux, C.P. 1020, Varennes, Québec, Canada, J3X 1S2*
[2]*IREQ, Hydro-Québec, C.P. 1000, Varennes, Québec, Canada, J3X 1S1*
*(*author for correspondence, e-mail: dodelet@inrs-ener.uquebec.ca)*

Received 14 December 1999; accepted in revised form 30 May 2000

Key words: mechanical alloying, PEFC, PEM fuel cell, process control agent, Pt–Ru alloy

Abstract

Ball-milling has been used to prepare performing CO tolerant polymer electrolyte fuel cell anode catalysts that contain Pt and Ru. The catalyst precursors are obtained by milling together Pt, Ru and a dispersing agent in the atomic ratio 0.5, 0.5 and 4.0. This precursor is not easily recovered after milling because it sticks to the walls of the vial and on the grinding balls. However, the precursor is recovered as a powder when a process control agent (PCA) is added during the milling step. Various PCAs have been used. The PCA should not interfere with the electrocatalytic activity of the catalysts obtained by leaching the precursor. The best preparation of catalyst precursors are obtained by milling: (i) Pt, Ru and Al (dispersing agent) in the atomic ratio 0.5, 0.5, 4.0 + 10 wt % NaF (PCA) or (ii) Pt , Ru and MgH_2 in the 0.5, 0.5, 4.0 atomic or molecular ratio. In this case, MgH_2 plays at the same time the role of a dispersing agent and that of a PCA. The catalysts are obtained by leaching Al and NaF in (i) or MgH_2 in (ii). The CO tolerance of these catalysts is equivalent to that of $Pt_{0.5}Ru_{0.5}$ Black from Johnson Matthey. The ball-milled catalysts have a surface area comprised between 30 and 44 $m^2\ g^{-1}$. As-prepared catalysts are mainly made of metallic Pt and metallic plus oxidized Ru. After fuel cell tests, Pt is completely metallic while the oxidized Ru content decreases but does not disappear. These catalysts are composed of particles with crystallites of two different sizes: in (i) nanocrystallites ($\sim$4 nm) that contain essentially Pt alloyed with Al and perhaps some Ru, and larger ($\geqslant\sim$30 nm) crystallites that contain essentially Ru; in (ii) Pt nanocrystalline particles that may contain some Ru and larger particles that contain essentially either Ru or Pt.

1. Introduction

Polymer electrolyte fuel cells are low temperature electrical generators using Pt-based electrocatalysts to activate both hydrogen electrooxidation and oxygen electroreduction [1]. When H_2 is obtained by reforming alcohols or hydrocarbons, the CO content of the hydrogen feedstream has to be lowered to a few ppm before entering the anode because pure Pt catalysts are prone to CO poisoning. Several Pt alloys, like Pt–Ru, Pt–Sn and Pt–Mo alloys, have been proposed to alleviate this poisoning problem (see, for instance, [2] and references therein) [3–5]. Among these alloys, Pt–Ru alloys are certainly the most studied catalysts mainly because their CO tolerance has been known for more than 30 years [6–8]. Pt–Ru alloys are also the main catalysts used at the anode of direct methanol fuel cells (DMFCs) [9–15]. This is again a consequence of CO poisoning since CO is also obtained by the consecutive dissociation electroadsorption steps of methanol at Pt electrodes [16–18].

Several methods have been used to prepare Pt–Ru catalysts for polymer electrolyte fuel cells. Recently [19], it was demonstrated that high energy ball-milling (or mechanical alloying), an industrially scalable technique, was able to produce unsupported catalysts containing Pt and Ru which show, in fuel cell tests, performance and CO tolerance equivalent to those of $Pt_{0.5}Ru_{0.5}$ Black commercially available from Johnson Matthey.

Mechanical alloying is an interesting low temperature alloying technique which is able to: (i) define alloy grain sizes down to the nanometer range; (ii) extend the solubility limits of one element into the other beyond thermodynamic equilibrium; (iii) synthesize new crystalline and quasicrystalline phases; (iv) develop amorphous phases; (v) produce disordered intermetallics; (vi) alloy difficult elements; and (vii) induce solid state reactions at low temperature [20].

The principle of high energy ball-milling is simple. A vial containing the powder to be milled and the grinding balls is secured in a clamp and swung energetically back and forth several thousand times a minute. With each swing of the vial, the balls impact at high velocity against the sample and the walls of the vials, both milling and mixing the sample. During this procedure,

the powder particles are repeatedly flattened, fractured and rewelded by the creation of new surfaces until grains of nanometric dimensions are obtained. It is clear that during mechanical alloying, heavy deformation is introduced into the particles. This is manifested by the presence of a variety of crystal defects that increase the diffusivity of solute elements into the matrix resulting in true alloying among the constituent elements.

This paper describes the technique of high energy ball-milling to the preparation of interesting catalysts for fuel cells using a protonic membrane, like PEM fuel cells and DMFCs. As it is easy to prepare unsupported catalysts by high energy ball-milling, this technique is particularly well adapted to the production of catalysts for DMFCs, for which large amounts (1–5 mg of metal cm^{-2}) of Pt and Pt–Ru alloys are used at the cathode and anode, respectively [9–15]. However, before using mechanical alloying to prepare novel catalysts for the anode of DMFCs, it is necessary to demonstrate that this technique is able to produce well known CO tolerant catalysts based on Pt and Ru or Pt and Mo. It is also necessary to demonstrate that important problems which are inherent to the high energy ball-milling technique may be solved.

One of the most important problem encountered in the use of mechanical alloying for the synthesis of performing Pt–Ru catalysts is the low specific area of the material obtained by milling Pt and Ru powders. Although a nanocrystalline structure was obtained and a true alloy was formed when Pt and Ru were milled together (for an initial ratio of Pt/Ru = 1, a Pt–Ru alloy having the $Pt_{0.48}Ru_{0.52}$ stoichiometry was obtained), the specific area of the alloy was only 0.45 $m^2\ g^{-1}$ [21]. This was due to the aggregation of Pt–Ru alloy nanoparticles in clusters of micrometric dimensions. The problem was solved by adding a third element, Al, to disperse Pt and Ru powders during the milling step. Afterwards, Al was leached in 1 M NaOH. Doing so, the specific area of the catalyst rose to 37.9 $m^2\ g^{-1}$, a value approaching that of $Pt_{0.5}Ru_{0.5}$ Black from Johnson Matthey (63.2 $m^2\ g^{-1}$). Both catalysts (milled and commercial) perform similarly in fuel cell tests under H_2 and H_2 + 100 ppm CO. However, the catalyst obtained by ball-milling was a composite of small (~4 nm) Pt particles alloyed with Al and perhaps some Ru and larger Ru particles [19].

Another important problem remains to be solved before using the ball-milling technique in the preparation of medium to large quantities of fuel cell catalysts. This problem is related to the fact that most of the ball-milled Pt–Ru composite catalyst remains stuck to the walls of the reaction vial and grinding balls instead of being recovered as a powder. In the present work, it will be demonstrated that the latter problem may be overcome by adding process control agents to the initial powder mixture of Pt, Ru and Al, the dispersive element. It will also be demonstrated that a process control agent like MgH_2, added to the initial powder mixture of Pt and Ru, is also able to play the role of the dispersing agent, eliminating the necessity to add Al.

2. Experimental details

2.1. *Catalyst preparation and characterization*

The various metal powders used in catalyst preparation were: Pt, <74 μm (−200 mesh) in size, 99.8% (Alfa Aesar); Ru, <44 μm (−325 mesh), 99.95% (Omega); Al, 44–420 μm (−40 + 325 mesh) (Johnson Matthey Electronics). The compounds used for process control agents were NaF, NaH, $LiAlH_4$, MgH_2, MgO, and $Mg(OH)_2$; except for MgH_2 (Tego Magnan), all chemicals were from Alfa Aesar. The catalysts were prepared using a Spex 8000 ball-mixer. Metal powders (~6 g) and WC balls were loaded in a 70 ml WC vial. The exact content of the vial will be specified in the Result section. The ball-to-powder weight ratio was always ~4/1. All powder handling was performed in an Ar-filled glove box, and the vial was hermetically sealed with a Viton O-ring. Milling times of 40 h were routinely used.

The ball-milled materials were characterized by (i) X-ray diffraction (XRD) using a Siemens D-500 diffractometer equipped with a CuK_α radiation source. The crystallite size was evaluated from the peak width at half height according to the procedure described by Cullity [22]; (ii) surface area measurements by N_2 adsorption (multipoint BET) using a Quantachrome Autosorb automated gas sorption system; (iii) neutron activation analysis to obtain bulk concentrations of metals milled; and (iv) X-ray photoelectron spectroscopy (XPS) using a VG Escalab 220i-XL equipped with an AlK_α monochromatic source.

2.2. *Electrochemical measurements*

The electrocatalytic performances of the catalysts were evaluated for pure H_2 (UHP, Praxair) and H_2 + 100 ppm CO (UHP, BOC Canada) in a GT60 GlobeTech fuel cell test station. The ink was usually prepared by sonicating for 20 min 40 mg of metal powder, 150 μl of a Nafion® 5 wt % solution (Aldrich), 400 μl of methanol (Fisher Scientific, ACS), and 60 μl of glycerine (Fisher Scientific, ACS). A volume of 305 μl of the ink was pipetted onto a 5 cm^2 uncatalysed ELAT backing layer from E-TEK which was then dried in a vacuum oven for 1 h at 75 °C. The resulting catalyst loading was 4 mg cm^{-2} with a catalyst/Nafion® weight ratio of 85/15. Unless otherwise specified, all fuel cell experiments have been performed with this anode catalyst loading, mainly to allow direct comparison with future experiments in DMFCs. Lower catalyst loadings (1 mg cm^{-2} and 0.5 mg cm^{-2} with a catalyst/Nafion® weight ratio of 50/50) have also been used. A Pt catalysed ELAT backing layer (E-TEK, 0.35 mg Pt cm^{-2}) painted with a 5 wt % Nafion® solution was used as the cathode.

After drying in a vacuum oven at 75 °C, the Nafion® deposited on the cathode amounted to 0.6 mg cm^{-2}.

Nafion 117® was used as the polymer electrolyte in the membrane electrode assembly. The membranes were cleaned by immersing them in boiling 3% H_2O_2 (Fisher Scientific, ACS) for 1 h. Then, they were rinsed with deionized water and immersed for 1 h in boiling 0.5 M H_2SO_4 (Fisher Scientific, ACS) followed by 1 h in boiling deionized water. The membrane electrode assembly was obtained by hot-pressing the Nafion 117® membrane between the anode and the cathode at 140 °C for 40 s under 2500 pounds. Current stabilization at 0.5 V was reached before recording the polarization curves. These were obtained under the following conditions: cell temperature 80 °C; temperature of water humidifying the anode and cathode gases 110 °C; H_2 (or H_2 + 100 ppm CO) pressure 30 psig; O_2 (UHP, Praxair) pressure = 60 psig. H_2 and O_2 flow rates 0.2 slm. For experiments involving CO, H_2 + 100 ppm CO was fed into the cell for 30 min under open circuit potential conditions before measuring the polarization curve.

Two commercial catalysts were used as references for the fuel cell tests; these were: Platinum Black (Fuel Cell Grade, Alfa AESAR, Johnson Matthey) (Pt Black (J.M.)); Platinum Ruthenium Black (Pt 66%, Ru 34% (w/w), Alfa AESAR, Johnson Mattey) ($Pt_{0.5}Ru_{0.5}$ Black (J.M.)).

3. Results and discussion

Figure 1 presents the polarization curves in H_2 + 100 ppm CO of Pt Black (J.M.) (□), $Pt_{0.5}Ru_{0.5}$ Black (J.M.) (○), and the ball-milled catalyst $Pt_{0.5}Ru_{0.5}(Al)_4$ (+) obtained by milling together Pt, Ru and Al in the atomic ratio 0.5: 0.5: 4.0, then leaching the milled material in a 1 M NaOH aqueous solution. The polarization curves in Figure 1 indicate that Pt Black is strongly poisoned while $Pt_{0.5}Ru_{0.5}$ Black and $Pt_{0.5}Ru_{0.5}(Al)_4$ show a similar CO tolerance. Although both Ru-containing catalysts display CO tolerance, their performance is lower than that in pure H_2. This is indicated by the polarization curve of $Pt_{0.5}Ru_{0.5}$ Black (dotted curve in Figure 1). The polarization curve of $Pt_{0.5}Ru_{0.5}(Al)_4$ in pure H_2 is similar to that of $Pt_{0.5}Ru_{0.5}$ Black but it is not displayed for the sake of clarity.

As stated in Section 1, when Pt, Ru and Al in the 0.5: 0.5: 4.0 atomic ratio are milled together, the resulting material sticks to the walls of the vial and on the grinding balls. This is due to the ductility of the metals and the cold welding properties of the milled particles. When this problem occurs in mechanical alloying, a process control agent (PCA) is added to the initial powder mixture. Usually, PCAs are organic compounds (stearic acid, hexane, oxalic acid, methanol, ethanol, acetone, heptane, octane, toluene, etc. [23]). They act as surface active agents, adsorbing on particule surfaces and interfering with cold welding by lowering the surface tension of the solid material. The majority of these compounds decompose and is incorporated in the powder particles during milling, resulting in the formation of carbides and oxides which are uniformly dispersed in the matrix [20].

In the present case, the milled Pt, Ru and Al are destined to be electrocatalysts for the oxidation of H_2. Therefore, it is necessary that the added PCA does not interfere with the electrocatalytic performance of the final material. Two solutions are proposed, both based on inorganic (instead of the usual organic) PCAs. In the first case, PCA is simply added to the Pt, Ru, and Al powders to be milled. In the second case, PCA is added to Pt and Ru powders to be milled; it will also play the dispersing role of Al which then becomes unnecessary.

3.1. *Addition of the process control agent (PCA) to Pt, Ru, and Al powders*

$LiAlH_4$, NaH and NaF have been used as process control agents. They were added as 10 wt % to the 6 g

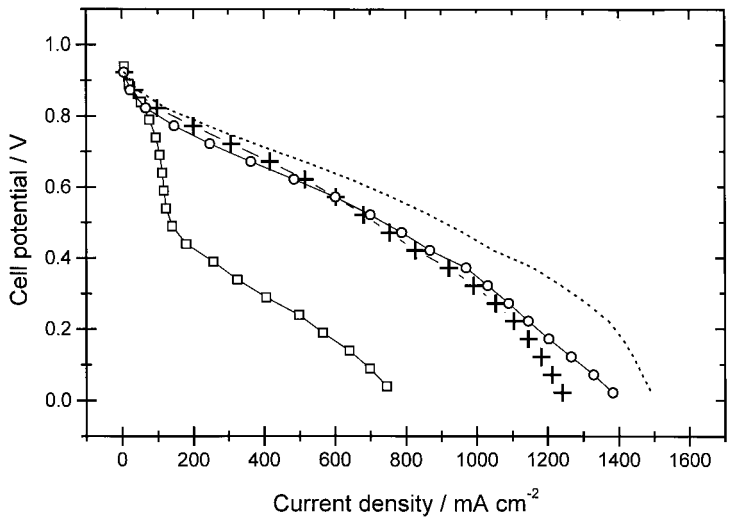

Fig. 1. Polarization curves in H_2 + 100 ppm CO of Pt Black (□), $Pt_{0.5}Ru_{0.5}$ Black (○) and the ball-milled catalyst $Pt_{0.5}Ru_{0.5}(Al)_4$ (+). Polarization curve of $Pt_{0.5}Ru_{0.5}$ Black in H_2 (- - - - -) is also shown.

of Pt, Ru, and Al powders in the 0.5: 0.5: 4.0 atomic ratio. A lower amount of NaF (5 wt %) was also used. In all cases, powders were obtained after 40 h of milling although a tendency to agglomeration was observed for 5 wt % NaF. The recovery of ball-milled material was close to 100% in all cases, compared to about 60% when no process control agent was used. To obtain the catalyst, the milled powder was first suspended in deionized water to dissolve PCA then NaOH was added to the suspension to leach Al. During this operation, both Al and PCA were dissolved. The catalysts were then rinsed with deionized water and dried.

Figure 2 presents the polarization curves in H_2 + 100 ppm CO for $Pt_{0.5}Ru_{0.5}$ $(Al)_4$ (+), $Pt_{0.5}Ru_{0.5}$ $(Al)_4$ + 5 wt % NaF (▲), $Pt_{0.5}Ru_{0.5}$ $(Al)_4$ + 10 wt % NaF (*), $Pt_{0.5}Ru_{0.5}$ $(Al)_4$ + 10 wt % NaH (♦), and $Pt_{0.5}Ru_{0.5}$ $(Al)_4$ + 10 wt % $LiAlH_4$ (●). Pt Black (□) and $Pt_{0.5}Ru_{0.5}$ Black (○) are given for comparison. It is obvious from Figure 2 that all PCAs at 10 wt % are not equivalent. NaF is the best one. This PCA does not affect the fuel cell performance of the $Pt_{0.5}Ru_{0.5}$ $(Al)_4$ catalyst. On the other hand, adding 10 wt % of $LiAlH_4$ removes all catalytic activity from $Pt_{0.5}Ru_{0.5}$ $(Al)_4$. There is also a difference in the performance when NaF is added at 5 wt % instead of 10 wt %.

All catalysts have been analyzed by BET, XPS and XRD in order to understand the effect of various PCAs on their performance. The specific area of the various $Pt_{0.5}Ru_{0.5}$ $(Al)_4$ catalysts obtained with and without PCA are given in Table 1, where, it is shown that: (i) the use of PCA always decreases the specific area of the catalyst; (ii) the performance of the catalyst are in the same order than their specific area, being maximum for 10 wt % NaF and minimum for 10 wt % $LiAlH_4$; (iii) the polarization curves of the $Pt_{0.5}Ru_{0.5}$ $(Al)_4$ type catalysts in H_2 + 100 ppm CO are similar to that of $Pt_{0.5}Ru_{0.5}$ Black as long as the specific area of the $Pt_{0.5}Ru_{0.5}$ $(Al)_4$ catalysts obtained with or without PCA is above ~30 m^2 g^{-1}.

Table 1. Effect of the process control agent, PCA, on the specific area and on the size of the Pt and Ru containing particles of the $Pt_{0.5}Ru_{0.5}$ $(Al)_4$-type catalysts

PCA /wt %	Specific area /m^2 g^{-1}	Crystallite size (Pt) /nm	Crystallite size (Ru) /nm
None	37.9	~4	~30
10% NaF	30.3	~4	~29
5% NaF	20.7	~6–10	~32
10% NaH	16.0	~16	~110
10% $LiAlH_4$	1.9	–	~30
$Pt_{0.5}Ru_{0.5}$ Black (J.M.)*	63.2	~3	–

* for comparison with a commercial reference

XRD results are presented in Figures 3 and 4. Figure 3 displays the X-ray diffractograms of $Pt_{0.5}Ru_{0.5}$ Black, $Pt_{0.5}Ru_{0.5}$ $(Al)_4$, $Pt_{0.5}Ru_{0.5}$ $(Al)_4$ + 10 wt % NaF and $Pt_{0.5}Ru_{0.5}$ $(Al)_4$ + 5 wt % NaF while Figure 4 presents the X-ray diffractograms of $Pt_{0.5}Ru_{0.5}$ $(Al)_4$ + 10 wt % NaF, $Pt_{0.5}Ru_{0.5}$ $(Al)_4$ + 10 wt % NaH, and $Pt_{0.5}Ru_{0.5}$ $(Al)_4$ + 10 wt % $LiAlH_4$. The vertical lines in both figures indicate the diffraction position of unalloyed (111) Pt at 2θ = 39.76°. The simplest diffractogram is that of $Pt_{0.5}Ru_{0.5}$ Black (Figure 3). It is composed of two broad and asymetric peaks in the 2θ range displayed. This asymetry indicates that $Pt_{0.5}Ru_{0.5}$ Black is not homogeneous but is composed of: (i) unalloyed or slightly alloyed large Pt crystallites diffracting at or near the position expected for pure Pt; and (ii) small crystallites of Pt–Ru alloy characterized by a broad diffraction peak shifted to higher 2θ values compared to pure Pt. According to our own work on Pt–Ru alloys prepared by ball-milling [21] and that of Gasteiger et al. [24] , the (111) planes of a $Pt_{0.5}Ru_{0.5}$ alloy should diffract at a peak situated at 40.39°, which is shifted 0.63° relative to the diffraction angle of unalloyed (111) Pt. The XRD spectrum of $Pt_{0.5}Ru_{0.5}$ Black has been deconvoluted into two narrow peaks at 2θ = 39.80 and 46.28° and two broad peaks at

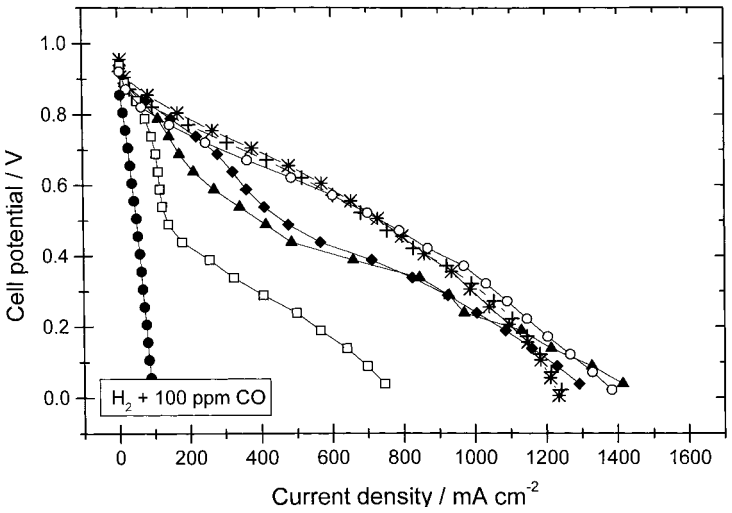

Fig. 2. Polarization curves in H_2 + 100 ppm CO of the ball-milled catalysts: $Pt_{0.5}Ru_{0.5}$ $(Al)_4$ (+), $Pt_{0.5}Ru_{0.5}$ $(Al)_4$ + 5 wt % NaF (▲), $Pt_{0.5}Ru_{0.5}$ $(Al)_4$ + 10 wt % NaF (*), $Pt_{0.5}Ru_{0.5}$ $(Al)_4$ + 10 wt % NaH (♦), and $Pt_{0.5}Ru_{0.5}$ $(Al)_4$ + 10 wt % $LiAlH_4$ (●). Pt Black (□) and $Pt_{0.5}Ru_{0.5}$ Black (○) are given for comparison.

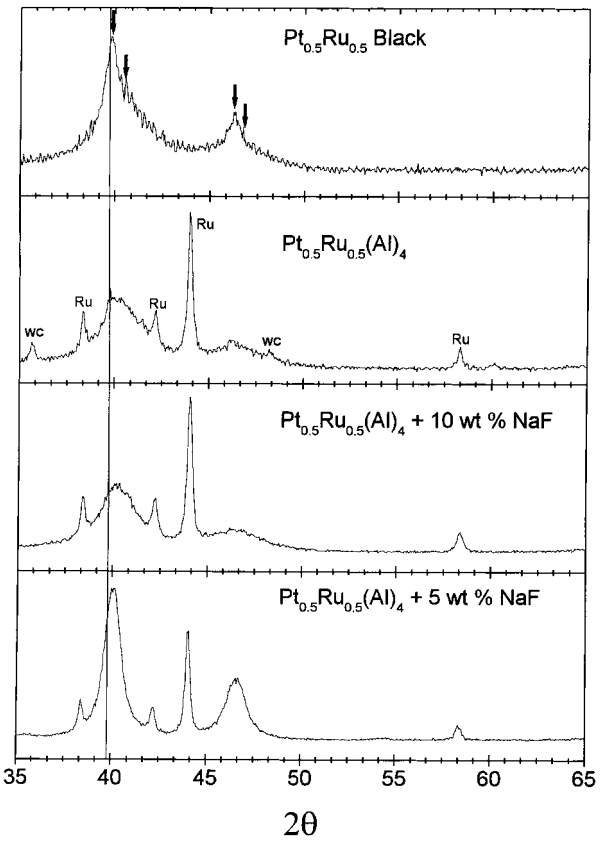

Fig. 3. XRD diffractograms of $Pt_{0.5}Ru_{0.5}$ Black and the ball-milled catalysts: $Pt_{0.5}Ru_{0.5}$ $(Al)_4$, $Pt_{0.5}Ru_{0.5}$ $(Al)_4$ + 10 wt % NaF and $Pt_{0.5}Ru_{0.5}$ $(Al)_4$ + 5 wt % NaF. The vertical line indicates the diffraction position of unalloyed (111) Pt. Arrows indicate the peak positions in the deconvolution of $Pt_{0.5}Ru_{0.5}$ Black.

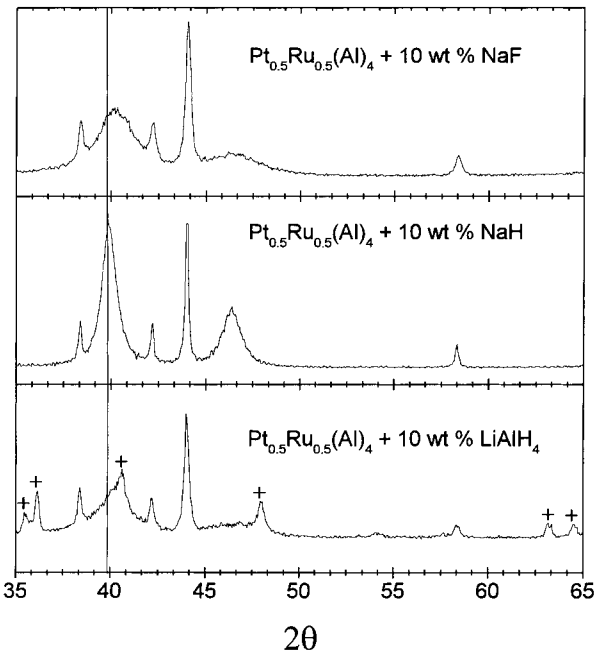

Fig. 4. XRD diffractograms of the ball-milled catalysts: $Pt_{0.5}Ru_{0.5}$ $(Al)_4$ + 10 wt % NaF, $Pt_{0.5}Ru_{0.5}$ $(Al)_4$ + 10 wt % NaH and $Pt_{0.5}Ru_{0.5}$ $(Al)_4$ + 10 wt % $LiAlH_4$. Vertical line indicates the diffraction position of unalloyed (111) Pt. In the diffractogram of $Pt_{0.5}Ru_{0.5}$ $(Al)_4$ + 10 wt % $LiAlH_4$ the peaks assigned to $LiAl(OH)_7 \cdot H_2O$ are identified by the symbol (+).

$2\theta = 40.53°$ and $46.85°$ (see arrows in Figure 3). A shift of 0.77° for (111) Pt corresponds to a $Pt_{0.39}Ru_{0.61}$ alloy which represents the maximum solubility of Ru into an f.c.c. Pt–Ru solid solution [21, 25].

The X-ray diffractogram of $Pt_{0.5}Ru_{0.5}$ $(Al)_4$ is similar to that of $Pt_{0.5}Ru_{0.5}$ $(Al)_4$ + 10 wt % NaF. It has already been reported [19] that $Pt_{0.5}Ru_{0.5}$ $(Al)_4$ is a composite catalyst made of small (~4 nm) crystallites of Pt alloyed with Al and perhaps some Ru, and of larger (~30 nm) Ru crystallites. The peaks belonging to Ru have been identified in Figure 3. Two peaks belonging to WC (from attrition of the vial and grinding balls) are also visible in the same diffractogram. $Pt_{0.5}Ru_{0.5}$ $(Al)_4$ + 10 wt % NaF has therefore the same composition than $Pt_{0.5}Ru_{0.5}$ $(Al)_4$. When the amount of NaF is decreased, the peaks belonging to Pt become narrower, indicating that the Pt–Al alloy crystallites are larger in $Pt_{0.5}Ru_{0.5}$ $(Al)_4$ + 5 wt % NaF than in $Pt_{0.5}Ru_{0.5}$ $(Al)_4$ + 10 wt % NaF. This catalyst remains a composite of small (~8 nm) crystallites of Pt alloyed with Al and perhaps some Ru, and of larger (~32 nm) Ru crystallites. The same conclusion is drawn for $Pt_{0.5}Ru_{0.5}$ $(Al)_4$ + 10 wt % NaH whose diffractogram is presented in Figure 4. In this case, the size of the Pt based crystallites is ~16 nm. All Pt and Ru crystallite sizes are reported in Table 1.

Finally, the XRD diffractogram of $Pt_{0.5}Ru_{0.5}$ $(Al)_4$ + 10 wt % $LiAlH_4$ comprises diffraction peaks belonging to $LiAl(OH)_7 \cdot H_2O$ (crosses in Figure 4) which remains in the catalyst structure after leaching the ball-milled material in NaOH. This compound is probably the cause of the low specific area of that catalyst and also its low performance in fuel cell tests. This catalyst was not considered for further characterizations.

Figure 5 presents the XPS spectra at the Pt 4f core levels of the following powders: $Pt_{0.5}Ru_{0.5}$ $(Al)_4$, $Pt_{0.5}Ru_{0.5}$ $(Al)_4$ + 10 wt % NaF, $Pt_{0.5}Ru_{0.5}$ $(Al)_4$ + 5 wt % NaF, and $Pt_{0.5}Ru_{0.5}$ $(Al)_4$ + 10 wt % NaH, before their use as anode catalysts in fuel cell. For the sake of comparison, equivalent spectra are also given for as-received Pt Black and $Pt_{0.5}Ru_{0.5}$ Black. The Pt 4f XPS spectrum of Pt Black is characteristic of metallic Pt. The Pt $4f_{5/2}$ and $4f_{7/2}$ peaks are both skewed towards higher binding energies as it is commonly observed at metallic surfaces. The $4f_{7/2}$ peak appears at 71.0 eV. It is the binding energy of Pt^0 [26]. There is a 3.35 eV gap between Pt $4f_{5/2}$ and $4f_{7/2}$ peaks. No Pt 4f contribution for $Pt(OH)_2$ (Pt $4f_{7/2}$ at 72.4 eV [26]) or PtO (Pt $4f_{7/2}$ at 73.8 eV [27]) is detected in the spectrum of Pt Black.

A vertical line has been drawn through the peak of Pt $4f_{7/2}$ of Pt Black to compare its peak position with that of the other catalysts. The only spectrum showing marked differences is that of $Pt_{0.5}Ru_{0.5}$ Black. First, there is a slight contribution of an oxidized Pt component which is mainly visible as a shoulder in the Pt $4f_{5/2}$

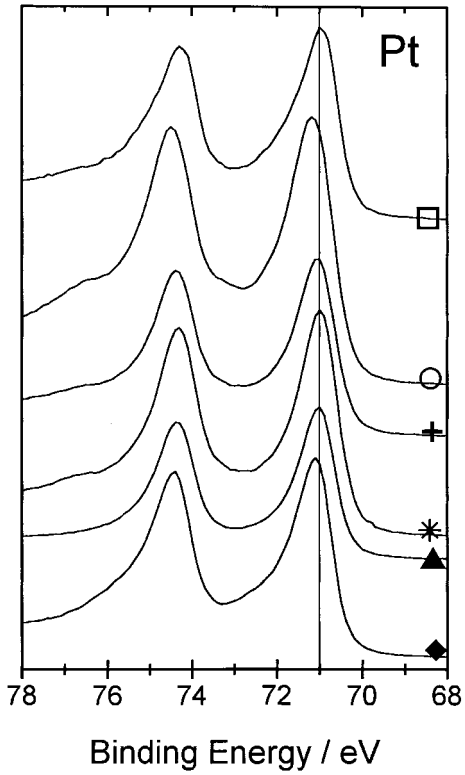

Fig. 5. XPS spectra at the Pt 4f core levels of the ball-milled catalysts: $Pt_{0.5}Ru_{0.5}$ $(Al)_4$ (+), $Pt_{0.5}Ru_{0.5}$ $(Al)_4$ + 10 wt % NaF (*), $Pt_{0.5}Ru_{0.5}$ $(Al)_4$ + 5 wt % NaF (▲) and $Pt_{0.5}Ru_{0.5}$ $(Al)_4$ + 10 wt % NaH (♦), before their use as anode catalysts in fuel cells. Pt Black (□) and $Pt_{0.5}Ru_{0.5}$ Black (○) are added for comparison. Vertical line indicates the peak position of metallic Pt.

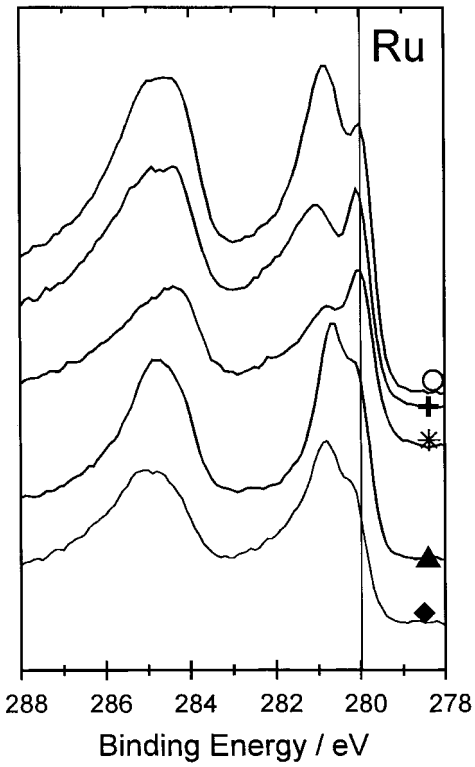

Fig. 6. XPS spectra at the Ru 3d core levels of the ball-milled catalysts: $Pt_{0.5}Ru_{0.5}$ $(Al)_4$ (+), $Pt_{0.5}Ru_{0.5}$ $(Al)_4$ + 10 wt % NaF (*), $Pt_{0.5}Ru_{0.5}$ $(Al)_4$ + 5 wt % NaF (▲) and $Pt_{0.5}Ru_{0.5}$ $(Al)_4$ + 10 wt % NaH (♦), before their use as anode catalysts in fuel cells. $Pt_{0.5}Ru_{0.5}$ Black (○) is added for comparison. Vertical line indicates the peak position of metallic Ru.

region above 76 eV. Secondly, there is a slight shift (0.2 eV) of both Pt 4f peaks towards higher binding energies. It has been shown that this core level shift is a result of alloying Pt and Ru [21]. Similar shifts to higher binding energies have also been reported when Pt is alloyed with Ti and Cr [28, 29]. From the results presented in Figure 5, it is concluded that Pt is mainly metallic in all $Pt_{0.5}Ru_{0.5}$ $(Al)_4$ -type catalysts and that a Pt–Ru alloy is probably not formed by ball-milling, at least to the extent existing in $Pt_{0.5}Ru_{0.5}$ Black, since the binding energy shift of all Pt 4f peaks belonging to $Pt_{0.5}Ru_{0.5}$ $(Al)_4$-type catalysts are either inexistant or marginal. This is in agreement with the XRD results where sharp Ru peaks are always detected for all $Pt_{0.5}Ru_{0.5}$ $(Al)_4$-type catalysts.

Figure 6 presents the XPS spectra at the Ru 3d core levels of the following powders: $Pt_{0.5}Ru_{0.5}$ $(Al)_4$, $Pt_{0.5}Ru_{0.5}$ $(Al)_4$ + 10 wt % NaF, $Pt_{0.5}Ru_{0.5}$ $(Al)_4$ + 5 wt % NaF, and $Pt_{0.5}Ru_{0.5}$ $(Al)_4$ + 10 wt % NaH, before their use as anode catalysts in fuel cell. For the sake of comparison, the equivalent spectra are also given for as-received $Pt_{0.5}Ru_{0.5}$ Black. The Ru $3d_{5/2}$ core level of metallic Ru peaks at 280.0 eV while that of RuO_2 is found at 280.7 eV [30].

The Pt/Ru atomic ratio at the surface of the catalyst has been evaluated by XPS. The results are given in Table 2 which shows that there is always more Pt than Ru at the surface of the materials but no trend could be found between the Pt/Ru ratio and the catalytic performance of the $Pt_{0.5}Ru_{0.5}$ $(Al)_4$ – type materials. A larger surface content of Pt vs Ru for $Pt_{0.5}Ru_{0.5}$ $(Al)_4$ type catalysts is in agreement with the fact that these catalysts are composite materials containing large Ru crystallites but only Pt–Al nanocrystallites with perhaps some Ru. Since XPS probes only a thin region of the material surface, a sizeable fraction of the photoelectrons generated by X-ray in the larger Ru crystallites is never able to escape the material and remains undetected.

Bulk analysis was performed on $Pt_{0.5}Ru_{0.5}$ $(Al)_4$ + 10 wt % NaF in order to determine its Pt, Ru and Al bulk contents. The results are given in Table 2 which shows that: (i) some Pt is lost in the leaching procedure; the Pt/Ru ratio of the actual catalyst is 0.84 instead of the nominal Pt/Ru ratio of 1.0; (ii) Al remains in the catalyst structure after leaching the ball-milled material. This has already been mentioned for $Pt_{0.5}Ru_{0.5}$ $(Al)_4$, for which a comparable Al content between 1 to 3 wt % was found. XPS spectra indicated that metallic and oxidized Al were present at the surface of $Pt_{0.5}Ru_{0.5}$ $(Al)_4$. In fuel cell tests it was demonstrated that $Pt_{0.5}Ru_{0.5}$ $(Al)_4$ was a stable catalyst losing only 240 ppm Al in the membrane after a 300 h test [19]. Al is therefore incorporated in $Pt_{0.5}Ru_{0.5}$ $(Al)_4$ and in $Pt_{0.5}Ru_{0.5}$ $(Al)_4$ + 10 wt % NaF either as small clusters

Table 2. Bulk metal content, bulk and surface Pt/Ru ratios for $Pt_{0.5}Ru_{0.5}$ $(Al)_4$ type catalysts and $Pt_{0.5}Ru_{0.5}$ $(PCA)_4$-type catalysts

Catalyst	Bulk content*/wt %				Pt/Ru ratio/at %	
	Pt	*Ru*	*Al*	*Mg*	*Bulk*	*Surface*
$Pt_{0.5}Ru_{0.5}$ $(Al)_4$	–	–	–	–	–	1.2–1.5
$Pt_{0.5}Ru_{0.5}$ $(Al)_4$ + 10 wt % NaF	57.7	35.4	2.93	–	0.84	2.4
$Pt_{0.5}Ru_{0.5}$ $(Al)_4$ + 5 wt % NaF	–	–	–	–	–	1.6
$Pt_{0.5}Ru_{0.5}$ $(Al)_4$ + 10 wt % NaH	–	–	–	–	–	2.2
$Pt_{0.5}Ru_{0.5}$ Black (J.M.)	–	–	–	–	–	1.1
$Pt_{0.5}Ru_{0.5}$ $(MgH_2)_4$	61.8	37.0	–	0.97	0.87	2.1
$Pt_{0.5}Ru_{0.5}$ $(MgO)_4$	–	–	–	–	–	2.6
$Pt_{0.5}Ru_{0.5}$ $(Mg(OH)_2)_4$	–	–	–	–	–	5.0

* accuracy of neutron activation results: ±5%

undetected by XRD and/or alloyed with Pt. Based on the shift of the diffraction peaks towards higher 2θ values, it has already been concluded that a Pt–Al alloy was obtained by milling Pt and Al powders in the 1:4 atomic ratio, then leaching Al. In the present case, assuming that all Al detected in $Pt_{0.5}$ $Ru_{0.5}$ $(Al)_4$ + 10 wt % NaF is alloyed with Pt, a $Pt_{0.73}Al_{0.27}$ would be reached.

3.2. *Addition of the process control agent (PCA) to only Pt and Ru*

MgH_2, MgO or $Mg(OH)_2$ have been used as process control agent and, at the same time, as dispersing agents. These compounds were added to the metal powders to obtain catalysts of the $Pt_{0.5}Ru_{0.5}$ $(PCA)_4$-type. In all cases, powders were recovered after 40 h milling. To obtain the catalyst, the milled powder was then leached in 1 M HCl. During this operation, PCA was dissolved. The catalyst was then rinsed with deionized water and dried.

Figure 7 presents the polarization curves in H_2 + 100 ppm CO for $Pt_{0.5}Ru_{0.5}$ $(MgH_2)_4$ (●), $Pt_{0.5}Ru_{0.5}$ $(MgO)_4$ (♦), and $Pt_{0.5}Ru_{0.5}$ $(Mg(OH)_2)_4$ (▼). $Pt_{0.5}Ru_{0.5}$ $(Al)_4$ (+), Pt Black (□), and $Pt_{0.5}Ru_{0.5}$ Black (○) are given for comparison. The best performance is obtained with $Pt_{0.5}Ru_{0.5}$ $(MgH_2)_4$. It is similar to what was obtained with $Pt_{0.5}Ru_{0.5}$ $(Al)_4$ + 10 wt % NaF (Figure 2) except at low current densities where higher cell voltages are measured with $Pt_{0.5}Ru_{0.5}$ $(Al)_4$ + 10 wt % NaF. All catalysts have also been analysed by BET, XRD and XPS to understand the effect of various PACs on the cell performance. The results obtained with this second procedure are quite similar to those obtained with the first one. The specific area of the various $Pt_{0.5}Ru_{0.5}$ $(PCA)_4$ -type catalysts are given in Table 3. As for the first procedure, there is an agreement between the importance of the specific area of the catalyst and its performance in fuel cell; the best catalyst being $Pt_{0.5}Ru_{0.5}$ $(MgH_2)_4$.

Fuel cell tests were also carried out with $Pt_{0.5}Ru_{0.5}$ $(MgH_2)_4$ loadings lower than 4 mg cm^{-2}, that is 1 and 0.5 mg cm^{-2}. Anode loadings of 1 mg cm^{-2} yielded exactly the same polarization curve in H_2 + 100 ppm CO than loadings of 4 mg cm^{-2}, while loadings of 0.5 mg cm^{-2} indicated some poisoning. The current state-of-the-art reformer based PEM fuel cells use supported catalysts with typical loadings in the range

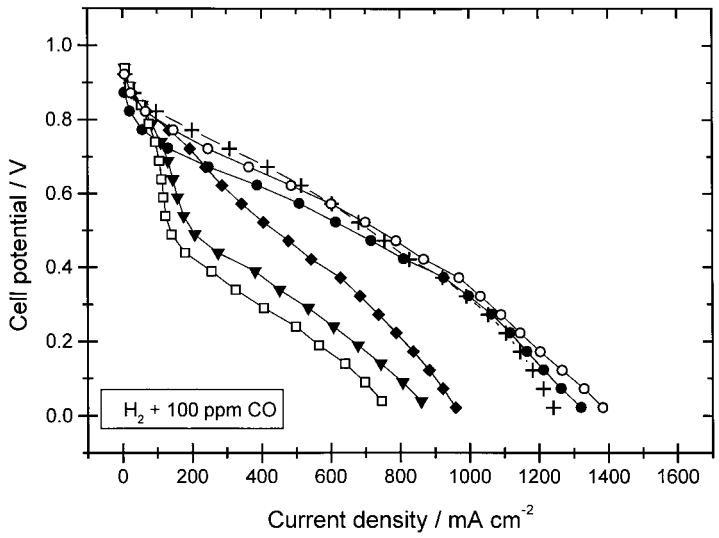

Fig. 7. Polarization curves in H_2 + 100 ppm CO for the ball-milled catalysts: $Pt_{0.5}Ru_{0.5}$ $(Al)_4$ (+), $Pt_{0.5}Ru_{0.5}$ $(MgH_2)_4$ (●), $Pt_{0.5}Ru_{0.5}$ $(MgO)_4$ (♦) and $Pt_{0.5}Ru_{0.5}$ $(Mg(OH)_2)_4$ (▼). Polarization curves for Pt Black (□) and $Pt_{0.5}Ru_{0.5}$ Black (○) are given for comparison.

Table 3. Effect of the process control agent (PCA), also acting as dispersing agent, on the specific area of $Pt_{0.5}Ru_{0.5}$ $(PCA)_4$

PCA	Specific area /$m^2\ g^{-1}$
MgH_2	44.1
MgO	23.9
$Mg(OH)_2$	6.1
$Pt_{0.5}Ru_{0.5}$ Black (J.M.)*	63.2

* for comparison with a commercial reference

of 0.9–0.3 mg cm^{-2}. The anode loading of 1 mg cm^{-2} necessary to obtain good polarization curves with $Pt_{0.5}Ru_{0.5}$ $(MgH_2)_4$ in H_2 + 100 ppm CO is therefore at the upper limit of the metal loading currently used in the PEM fuel cell industry.

Figure 8 presents the XRD diffractograms of $Pt_{0.5}Ru_{0.5}$ $(MgH_2)_4$, $Pt_{0.5}Ru_{0.5}$ $(MgO)_4$, and $Pt_{0.5}Ru_{0.5}$ $(Mg(OH)_2)_4$. The diffractograms of $Pt_{0.5}Ru_{0.5}$ Black and $Pt_{0.5}Ru_{0.5}$ $(Al)_4$ are given for comparison. From the diffractogram of $Pt_{0.5}Ru_{0.5}$ $(MgH_2)_4$, one may conclude that it is composed of three kinds of particles: small Pt crystallites and larger Pt and Ru grains, while $Pt_{0.5}Ru_{0.5}$ $(Mg(OH)_2)_4$ is made only of large Pt and Ru particles. Except for $Pt_{0.5}Ru_{0.5}$ $(Mg(OH)_2)_4$, none of the (111) Pt peaks in Figure 8 coincide with the unalloyed (111) Pt peak position (vertical line). Some Pt alloying is therefore expected. In the case of $Pt_{0.5}Ru_{0.5}$ $(PCA)_4$-type catalysts, only alloys with Ru and Mg are possible. The presence of unleached Mg has been checked in $Pt_{0.5}Ru_{0.5}$ $(MgH_2)_4$. The result (0.97 wt %) is reported in Table 2. Some metallic Mg might be obtained by the partial decomposition of MgH_2 during the milling process.

Figure 9 presents the XPS spectra at the Pt 4f core level of all $Pt_{0.5}Ru_{0.5}$ $(PCA)_4$-type powders before being used as anode catalysts in fuel cell. As-received Pt Black and $Pt_{0.5}Ru_{0.5}$ Black are also given for comparison. Pt is metallic in all $Pt_{0.5}$ $Ru_{0.5}$ $(PCA)_4$ type catalysts. The vertical line drawn through the peak of Pt $4f_{7/2}$ of Pt Black allows comparison of its peak position to that of the other catalysts. The only spectra showing a binding energy shift are those of $Pt_{0.5}Ru_{0.5}$ Black and $Pt_{0.5}Ru_{0.5}$ $(MgO)_4$. As mentioned previously, the shift in binding energy for $Pt_{0.5}Ru_{0.5}$ Black is the result of alloying Pt and Ru. The same reason may be invoked for $Pt_{0.5}Ru_{0.5}$ $(MgO)_4$. This is indeed corroborated by its XRD spectrum (Figure 8) where the main (111) Pt line is shifted towards larger 2θ values than all other $Pt_{0.5}Ru_{0.5}$ $(PCA)_4$.

Figure 10 presents the XPS spectra of the Ru 3d core level of all $Pt_{0.5}Ru_{0.5}$ $(PCA)_4$ type powders before being used as anode catalyst in fuel cell. The equivalent spectra are also given for as-received $Pt_{0.5}Ru_{0.5}$ Black and for $Pt_{0.5}Ru_{0.5}$ $(Al)_4$ powder. Metallic Ru is present in all catalysts. On the other hand, $Pt_{0.5}Ru_{0.5}$ $(MgO)_4$ and particularly $Pt_{0.5}Ru_{0.5}$ $(Mg(OH)_2)_4$ are characterized by a low Ru oxide/hydroxide content, which

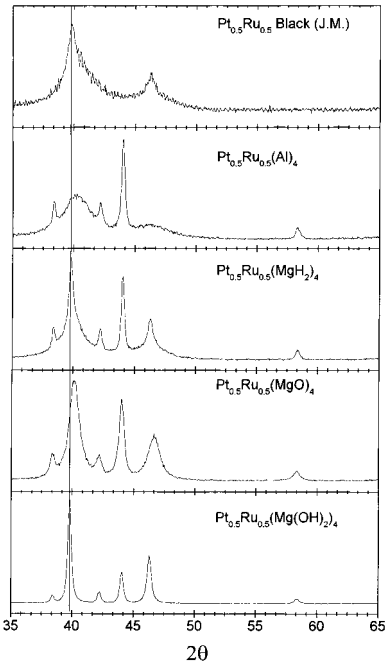

Fig. 8. XRD diffractograms of $Pt_{0.5}Ru_{0.5}$ Black and of the ball-milled catalysts: $Pt_{0.5}Ru_{0.5}$ $(Al)_4$, $Pt_{0.5}Ru_{0.5}$ $(MgH_2)_4$, $Pt_{0.5}Ru_{0.5}$ $(MgO)_4$ and $Pt_{0.5}Ru_{0.5}$ $(Mg(OH)_2)_4$. Vertical line indicates the diffraction position of unalloyed (111) Pt.

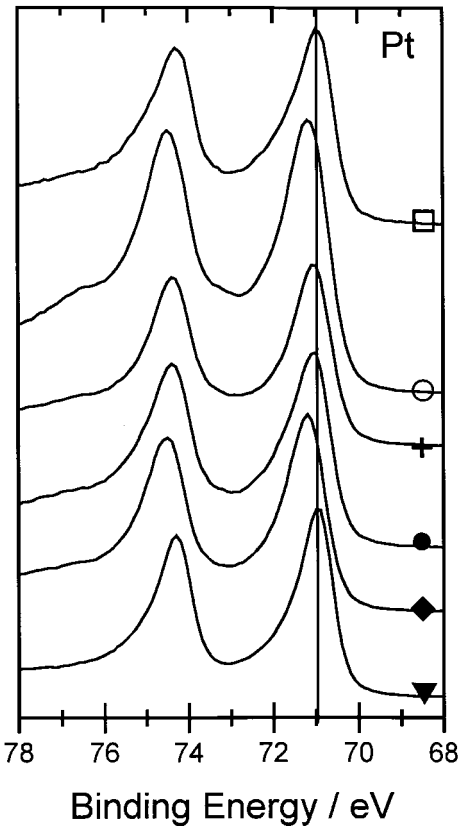

Fig. 9. XPS spectra at the Pt 4f core levels of the ball-milled catalysts: $Pt_{0.5}Ru_{0.5}$ $(MgH_2)_4$ (●), $Pt_{0.5}Ru_{0.5}$ $(MgO)_4$ (♦) and $Pt_{0.5}Ru_{0.5}$ $(Mg(OH)_2)_4$ (▼). Pt Black (□), $Pt_{0.5}Ru_{0.5}$ Black (○) and $Pt_{0.5}Ru_{0.5}$ $(Al)_4$ (+) are added for comparison. Vertical line indicates the peak position of metallic Pt.

appears at ~280.7 eV. These catalysts also behave poorly in fuel cells. It has been demonstrated [2, 31], using well characterized Pt–Ru alloys, that surface atoms of Ru provide the nucleation sites for the adsorption of oxygen containing species that are necessary for the oxidation of adsorbed CO. The reactions involved are:

$$Ru + H_2O \leftrightarrow Ru(OH)_{ads} + H^+ + e^- \quad (1)$$

$$(CO)_{ads} + (OH)_{ads} \rightarrow CO_2 + H^+ + e^- \quad (2)$$

The occurrence of an oxidized Ru in the XPS spectrum is therefore expected. A more drastic point of view on the importance of hydrous ruthenium oxide (RuO_xH_y) in Pt–Ru Blacks has been recently expressed by Rolinson et al. [32]. According to these authors, RuO_xH_y is a necessary species in the good operation of these catalysts.

It is possible that the presence of surface oxide species on Pt or on Ru in the as-prepared or as-received electrocatalysts does not necessary correlate with the situation near the typical hydrogen overpotential of 100–150 mV in H_2 + 100 ppm CO. XPS experiments were therefore performed on three catalysts ($Pt_{0.5}Ru_{0.5}(Al)_4$ + 10 wt % NaF, $Pt_{0.5}Ru_{0.5}(MgH_2)_4$, and $Pt_{0.5}Ru_{0.5}$ Black) immediately after completion of the fuel cell tests (20 h in H_2/O_2 followed by 20 h in H_2 + 100 ppm CO/O_2 at a constant potential of 0.5 V). In order to do so, the MEA was soaked in methanol; the anode was pealed from the membrane, dried in a vacuum oven at 75 °C for 20 min, and directly analyzed by XPS. The results obtained for Pt 4f are displayed in Figure 11, while those obtained for Ru $3d_{5/2}$ (peaks of Ru $3d_{3/2}$ of the catalyst and C1s of the membrane overlap) are displayed in Figure 12. Figure 11 reveals on one hand that any Pt oxide content

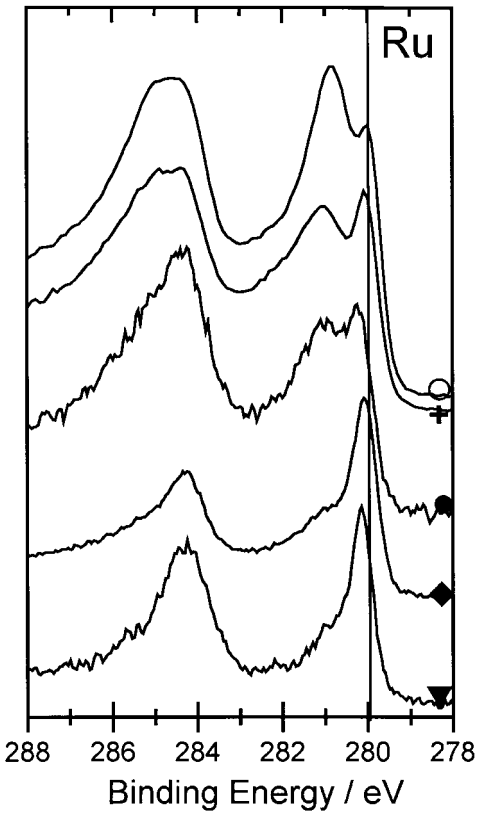

Fig. 10. XPS spectra at the Ru 3d core levels of the ball-milled catalysts: $Pt_{0.5}Ru_{0.5}(MgH_2)_4$ (●), $Pt_{0.5}Ru_{0.5}(MgO)_4$ (♦) and $Pt_{0.5}Ru_{0.5}(Mg(OH)_2)_4$ (▼). $Pt_{0.5}Ru_{0.5}$ Black (○) and $Pt_{0.5}Ru_{0.5}(Al)_4$ (+) are added for comparison. Vertical line indicates the peak position of metallic Ru.

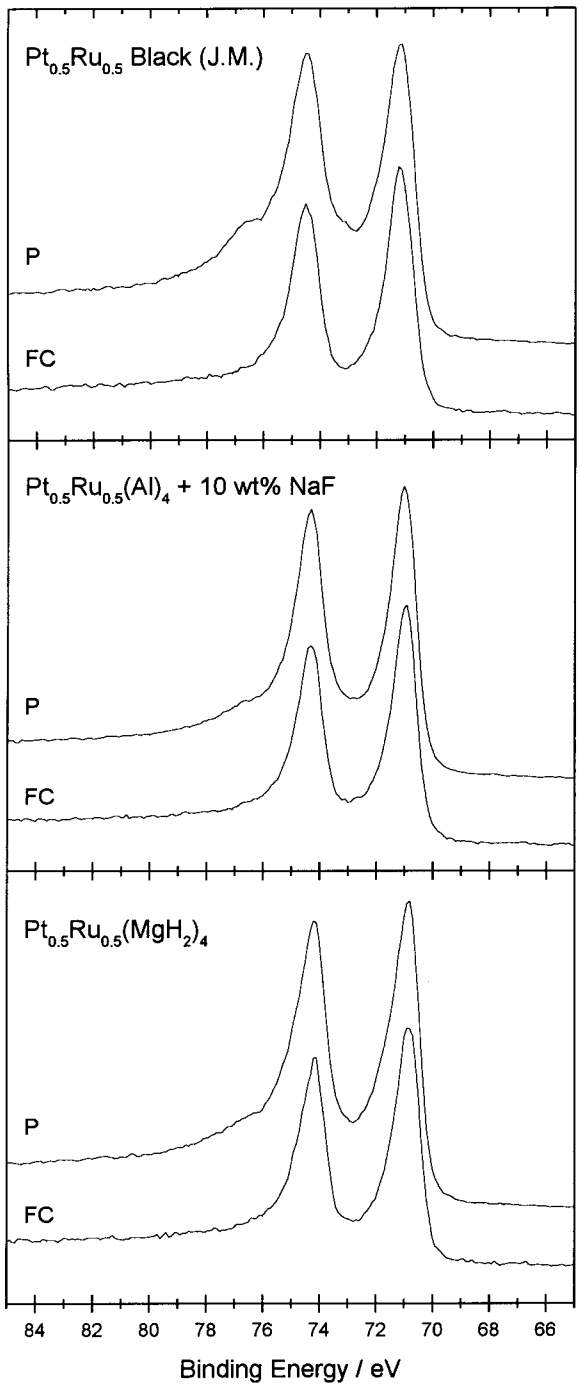

Fig. 11. XPS spectra at the Pt 4f core levels of $Pt_{0.5}Ru_{0.5}$ Black, $Pt_{0.5}Ru_{0.5}(Al)_4$, and $Pt_{0.5}Ru_{0.5}(MgH_2)_4$, before (P) and after fuel cell tests (FC).

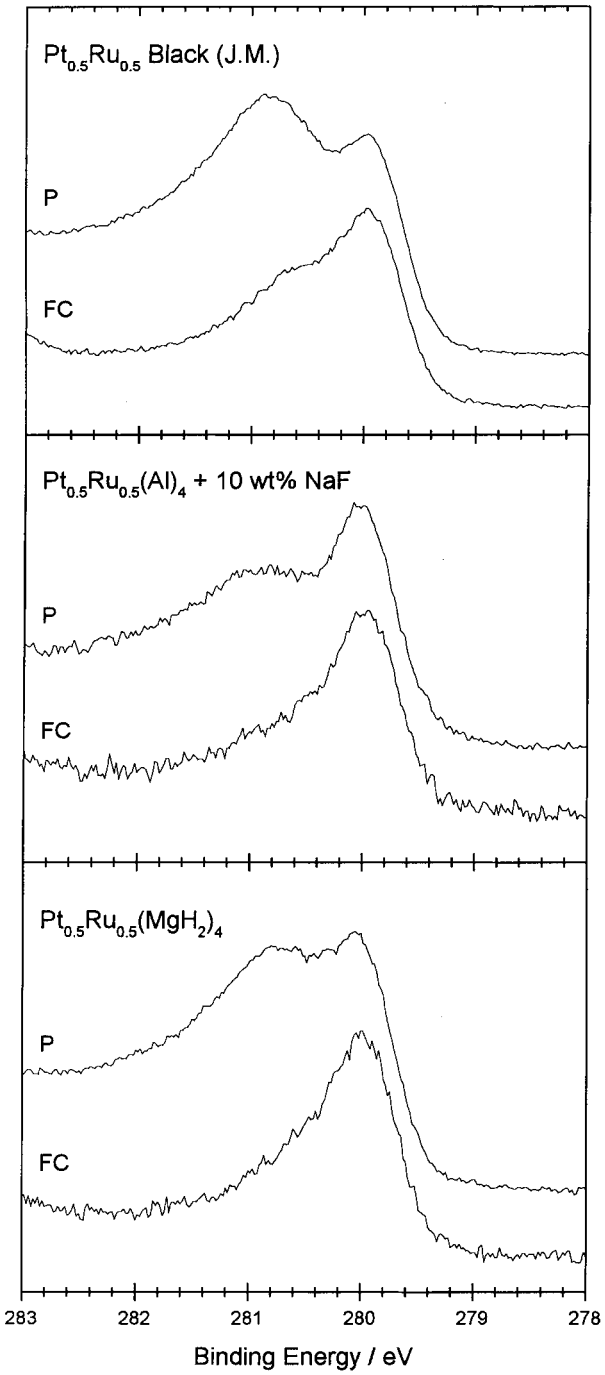

Fig. 12. XPS spectra at the Ru $3d_{5/2}$ core levels of $Pt_{0.5}Ru_{0.5}$ Black, $Pt_{0.5}Ru_{0.5}$ $(Al)_4$, and $Pt_{0.5}Ru_{0.5}$ $(MgH_2)_4$, before (P) after fuel cell tests (FC).

that was detected in the powder (see the shoulder above 76 eV) completely disappeared after the fuel cell test. On the other hand, Figure 12 shows that the broad oxide/hydroxide Ru $3d_{5/2}$ peak or shoulder (at ~280.7 eV) characteristic of the powder decreased but did not completely disappear. We believe that the smaller Ru oxide/hydroxide content seen in Figure 12 is also present during the fuel cell test and is not the result of a later reoxidation of Ru at the electrode surface. Indeed, it has been shown by XPS [33], that metallic Ru obtained after reduction of a Ru wafer in H_2 at 350 °C for 4 h does not reoxidize immediately after oxygen adsorption at room temperature.

4. Conclusions

It has been demonstrated that the addition of a process control agent during the milling of Pt and Ru based catalysts produce easily recovered powders. All compounds used as PCA are operating but do not yield equivalent CO tolerant anode catalysts for polymer electrolyte fuel cells. The best results are obtained with $Pt_{0.5}Ru_{0.5}$ $(Al)_4$ + 10 wt % NaF and $Pt_{0.5}Ru_{0.5}$ $(MgH_2)_4$. In both cases, PCA acts during milling without modifying significantly the catalytic performance. For these catalysts, BET, XRD and XPS characterizations indicate the following details.

(i) Their specific area is approximately the same than without PCA.

(ii) The oxidation state of Pt and Ru of the catalyst powders before fuel cell tests is the same than without PCA: mainly metallic Pt, but metallic and oxidized Ru are detected. After fuel cell tests, Pt is completely metallic and the oxidized Ru content decreases but does not disappear.

(iii) The composite structure of the catalysts is preserved. Both $Pt_{0.5}Ru_{0.5}$ $(Al)_4$ + 10 wt % NaF, $Pt_{0.5}Ru_{0.5}$ $(MgH_2)_4$ and $Pt_{0.5}Ru_{0.5}$ $(Al)_4$ made without PCA are composed of small Pt nanocrystallites but larger Ru particles. The small (~4 nm) crystallites of $Pt_{0.5}Ru_{0.5}$ $(Al)_4$ + 10 wt % NaF are made of a Pt-Al alloy, perhaps containing Ru. On the other hand, for $Pt_{0.5}Ru_{0.5}$ $(MgH_2)_4$, based on previous results where Pt, Ru, and Mg powders were milled together [19], it is believed that substitution of Pt with Mg on lattice sites for the small Pt crystallites is minimal but that alloying with small amounts of Ru remains a possibility.

The fact that a catalyst like $Pt_{0.5}Ru_{0.5}$ $(Al)_4$ + 10 wt % NaF is performing well in H_2 + 100 ppm CO is quite difficult to understand in the frame of reactions (1) and (2) reported in the Result and Discussion section. Indeed, for that catalyst Pt is alloyed with Al, while Ru is essentially present as another phase. Both metallic and oxidized Al and Ru are, however, detected on the surface of that catalyst. If there is no interaction between the Pt and Ru containing phases, it is expected that oxidized Al at the surface of Pt–Al nanocrystallites becomes the source of the oxygen containing species required for the oxidation of CO. Such a conclusion is similar to that of Rolinson et al. [32], stating that RuO_xH_y is the source of CO tolerance for Pt–Ru Blacks. On the other hand, if an interaction exists between the Pt and Ru phases, the possible migration of $(CO)_{ads}$ on the Pt surface [34, 35] will bring CO to the special spots where Pt surface atoms of the small Pt containing particles , on one side, are in contact with Ru surface atoms of the larger Ru containing particles, on the other side. There, Reaction 2 will

proceed. This conclusion is similar to that of Lin et al. [31] stating that electrooxidation of CO on well organized Ru islands on (111) Pt surfaces takes place preferentially at the Ru islands while CO adsorbed on Pt migrates on them. Other CO tolerant anode composite catalysts are also known (see for instance: Pt–Ru/WO_3 [36], Pt/WO_3 [37], Pt–Sn [38], Pt–Ru [39], and Pt-transition metal alloy-bronze forming element [40]). Further studies are needed to ascertain the CO tolerance mechanism of these catalysts.

References

1. S. Gottesfeld and T. A. Zawodzinski, *Adv. Electrochem. Sci. Eng.* **5** (1997) 195.
2. P.N. Ross, Jr., In J. Lipkowski and P.N. Ross (Eds), 'Electrocatalysis' (Wiley-VCH, New York, 1998), p. 43.
3. B.N. Grgur, N.M. Markovic and P.N. Ross, Jr., *J. Phys. Chem. B* **102** (1998) 2494.
4. B.N. Grgur, M. Markovic and P.N. Ross, *J. Electrochem. Soc.* **146** (1999) 1613.
5. S. Mukerjee, S.J. Lee, E.A. Ticianelli, J. McBreen, B.N. Grgur, N.M. Markovic, P.N. Ross, J.R. Giallombardo and E.S. De Castro, *Electrochem. Solid-State Lett.* **2** (1999) 12.
6. L.W. Niedrach, D.W. McKee, J. Paynter and I.F. Danzig, *J. Electrochem. Technol.* **5** (1967) 318.
7. D.W. McKee and A. Scarpellino, *J. Electrochem. Technol.* **6** (1968) 101.
8. P.N. Ross, K. Kinoshita, A.J. Scarpellino and P. Stonehart, *J. Electroanal. Chem.* **63** (1975) 97.
9. A.K. Shukla, P.A. Christensen, A.J. Dickinson and A. Hamnett, *J. Power Sources* **76** (1998) 54.
10. A.S. Arico, A.K. Shukla, K.M. El-Khatib, P. Creti and V. Antonucci, *J. Appl. Electrochem.* **29** (1999) 671.
11. M. Baldauf and W. Preidel, *J. Power Sources* **84** (1999) 161.
12. X. Ren, T. E. Springer and S. Gottesfeld, *J. Electrochem. Soc.* **147** (2000) 92.
13. H. Dohle, J. Divisek and R. Jung, *J. Power Sources* **86** (2000) 469.
14. X. Ren, P. Zelenay, S. Thomas, J. Davey and S. Gottesfeld, J. *Power Sources* **86** (2000) 111.
15. P. Argyropoulos, K. Scott and W.M. Taama, *J. Power Sources* **87** (2000) 153.
16. M.P. Hogarth and G. Hards, *Platinum Metals Rev.* **40** (1996) 150.
17. A. Hamnett, *Catalysis Today* **38** (1997) 445.
18. S. Wasmus and A. Küver, *J. Electroanal. Chem.* **461** (1999) 14.
19. M.C. Denis, G. Lalande, D. Guay, J.P. Dodelet and R. Schulz, *J. Appl. Electrochem.* **29** (1999) 951.
20. C. Suryanarayana, *in* C. Suryanarayana (Ed) 'Non-equilibrium Processing of Materials' (Pergamon Materials Series, Pergamon, Amsterdam, 1999) p. 49.
21. G. Lalande, M.C. Denis, D. Guay, J.P. Dodelet and R. Schulz, *J. Alloys Compounds* **292** (1999) 301.
22. B.D. Cullity, *in* 'Elements of X-ray Diffraction' (Addison-Wesley, 4th edn, 1978).
23. C. Suryanarayana, *in* P.W. Lee (Ed), 'Powder Metal Technologies and Applications' (ASM International, Materials Park, OH, 1998), p. 80.
24. H.A. Gasteiger, P.N. Ross and E.J. Cairns, *Surf. Sci.* 293 (1993) 67.
25. J.M. Hutchinson, *Plat. Met. Rev.* **16** (1972) 88.
26. J.S. Hammond and N. Winograd, *J. Electroanal. Chem.* **78** (1977) 55.
27. J.B. Goodenough, A. Hamnett, B.J. Kennedy, R. Manoharan and S.A. Weeks, *J. Electroanal. Chem.* **240** (1988) 133.
28. G.N. Derry and P.N. Ross, *Solid State Commun.* **52** (1984) 151.
29. K.A. Daube, M.T. Paffett, S. Gottesfeld and C.T. Campbell, *J. Vac. Sci. Technol. A* **4** (1986) 1617.
30. C.D. Wagner, W.W. Riggs, L.E. Davis, J.F. Moulder and G.E. Muilenberg, 'Handbook of X-ray Photoelectron Spectroscopy' (Perkin-Elmer Corporation, 1978).
31. W.F. Lin, M.S. Zei, M. Eiswirth, G. Ertl, T. Iwasita and W. Vielstich, *J. Phys. Chem. B* **103** (1999) 6968.
32. D.R. Rolinson, P.L. Hagans, K.E. Swider and J.W. Long, *Langmuir* **15** (1999) 774.
33. J.Y. Shen, A. Adnot and S. Kaliaguine, *Appl. Surf. Sci.* **51** (1991) 47.
34. M.T.M. Koper, J.J. Lukkien, A.P.J. Jansen and R.A. van Santen, *J. Phys. Chem. B* **103** (1999) 5522.
35. K.A. Friedrich, K.P. Geyzers, A. Marmann, U. Stimming and R. Z. Vogel, *Z. Phys. Chem.* **208** (1999) 137.
36. P.K. Shen, K.Y. Chen and A.C.C. Tseung, *J. Electrochem. Soc.* **142** (1995) L85.
37. G. Lalande, M.C. Denis, P. Gouerec, D. Guay, J.P. Dodelet and R. Schulz, *J. New Mater. Electrochem. Syst.* **3** (2000) 185.
38. F. Delime, J.M. Léger and C. Lamy, *J. Appl. Electrochem.* **29** (1999) 1249.
39. J. McBreen and S. Mukerjee, *J. Electrochem. Soc.* **142** (1995) 3399.
40. A. G. Gunner, I.T. Hyde, R.J. Potter and D. Thompsett, European Patent Application *EP 0838872A2*.